INFLUENCE OF THE NOZZLE-EXIT BOUNDARY-LAYER THICKNESS ON THE NOISE PRODUCED BY SUBSONIC IMPINGING JETS

Hugo Vincent, Christophe Bogey

DOI: 10.61782/fa.2023.0335

forum acusticum 2023

INFLUENCE OF THE NOZZLE-EXIT BOUNDARY-LAYER THICKNESS ON THE NOISE PRODUCED BY SUBSONIC IMPINGING JETS

Hugo Vincent* **Christophe Bogey**

Univ Lyon, Ecole Centrale de Lyon, CNRS, Univ Claude Bernard Lyon 1, INSA Lyon, LMFA, UMR5509, 69130, Ecully, France

ABSTRACT

The influence of the nozzle-exit boundary-layer thickness on the noise produced by initially laminar subsonic impinging jets is investigated using large-eddy simulations. For that purpose, six round jets at Mach numbers of 0.6 or 0.9, with nozzle-exit boundary-layer thickness equal to $0.05r_0$, $0.1r_0$ or $0.2r_0$, where r_0 is the pipe-nozzle radius, are considered. They impinge on a plate located at $6r_0$ from the nozzle-exit plane. For the jets at a Mach number of 0.9, the near-nozzle pressure spectra exhibit tones, at similar frequencies in all cases. However, for a thicker boundary layer, the dominant tone is nearly 30 dB stronger. The gain in amplitude of the shear-layer instability waves developing at its frequency between the nozzle and the plate also increases for thicker boundary layers. This indicates that the rise of the peak amplitude is the result of a higher amplification of the shear-layer instability waves. For the jets at a Mach number of 0.6, a large low-frequency hump and weak narrow peaks are found in the near-nozzle pressure spectrum for the thickest boundary layers, while no peaks are observed in the other cases. This suggests that impinging jets at Mach number lower than 0.65 can become resonant as their boundary layers are thicker.

Keywords: *impinging jet, nozzle-exit conditions, jet noise, feedback loop, large-eddy simulation*

**Corresponding author*: *hugo.vincent@ec-lyon.fr.*

1. INTRODUCTION

Strong acoustic tones are produced when highly subsonic or supersonic jets impinge on a plate [1–5]. Numerous studies have shown that these tones are due to aeroacoustic feedback loops establishing between the jet nozzle and the plate. The feedback loops consist of downstream-propagating shear-layer instability waves and upstream-travelling acoustic waves. Their different parts are detailed in the recent review by Edgington-Mitchell [6].

The downstream part of the feedback loops is well known. It involves large-scale coherent structures which are formed through the amplification of shear-layer instability waves along the jet mixing layers. Tam & Ahuja [7] and, afterwards, many authors [8,9] demonstrated that the upstream-travelling waves closing the feedback loops are acoustic modes of the jets. These modes have been first studied in detail by Tam & Hu [10] by modeling jets as annular vortex sheets of infinite length. They are only allowed in narrow frequency bands and share similarities with duct modes. The waves are mainly confined inside the jet column and are thus called guided jet waves in recent papers.

The effects of the Mach number and of the nozzle-to-plate distance on the tone frequencies have been documented in previous studies [3,11]. For a jet at a given Mach number, the tone frequency decreases as the nozzle-to-plate distance increases, and suddenly increases discontinuously for certain nozzle-to-plate distances [1,4], exhibiting a mode staging phenomenon typical of those observed in resonant flows with feedback loops. For jets at Mach numbers lower than 0.65, no tones are found in the acoustic spectra [5,11], whereas this is the case for jets at higher

Mach numbers. The tone frequencies decrease as the Mach number increases [3, 11]. For impinging jets at a given Mach number, Tam & Ahuja [7] showed that the mean tone frequency, determined by averaging the tone frequencies obtained for different nozzle-to-plate distances, corresponds to the lowest frequency of the least-dispersed guided jet waves. The latter frequency increases as the Mach number decreases, which allowed Tam & Ahuja [7] to explain the absence of tones for impinging jets at Mach numbers lower than 0.65 by pointing out that, for these Mach numbers, the lowest frequency of the least-dispersed guided jet waves is too high compared with the frequency of the most amplified shear-layer instability waves between the nozzle and the plate.

The tone frequencies obtained in two separate experiments for a given nozzle-to-plate distance also differ in some cases. For example, for a jet at a Mach number of 0.8 impinging on a plate located at four nozzle diameters from the nozzle-exit plane, Jaunet *et al.* [3] reported a tone at a frequency lower than the one measured by Panickar & Raman [8]. In some cases, differences are also found between the tone frequencies obtained in high-fidelity numerical simulations and in experiments. This can be observed, for instance, for the tone frequencies reported recently in the numerical study by Varé & Bogey [11] and those measured by Jaunet *et al.* [3]. The differences are often attributed to the nozzle-exit conditions (boundary-layer profile and initial turbulence level), not always known in the experiments. For free jets, it has been found, for instance, that the nozzle-exit conditions have a strong influence on the flow and noise of the jets [12, 13]. In particular, the frequency and growth rate of the shear-layer instability waves developing near the nozzle of jets with laminar boundary layers decrease for thicker boundary layers [12, 19].

To the best of the authors' knowledge, the effects of the nozzle-exit conditions on the noise produced by impinging jets have not been described yet. They are, however, likely to be significant. Indeed, since the properties of the shear-layer instability waves vary with the nozzle-exit conditions in free jets [12, 13, 19], the gain in amplitude of the instability waves between the jet nozzle and the plate, and consequently, the amplitudes of the tones found in impinging jets, are also expected to vary with the nozzle-exit conditions. Furthermore, for a jet at a Mach number lower than 0.65, the frequency of the shear-layer instability waves and of the least-dispersed guided jet waves are closer to each other for thicker boundary layers, which could enable the establishment of feedback loops.

Given the above, the influence of the nozzle-exit boundary-layer thickness on the noise generated by subsonic impinging jets is investigated in the present study. The first objective is to estimate the dependence of the tone frequencies and amplitudes on the nozzle-exit boundary-layer thickness for an impinging jet at a Mach number of 0.9. The second objective is to evaluate the effects of the boundary-layer thickness on the amplification of the shear-layer instability waves between the nozzle and the plate. A third objective is to determine whether feedback loops can happen for jets at a Mach number lower than 0.65.

The study is conducted by analyzing the flow and noise of six initially laminar impinging round jets at Mach numbers of 0.6 or 0.9 computed using large-eddy simulations. The jets impinge on plate located at 6 nozzle radii from the nozzle-exit plane. Their nozzle-exit boundary layers have thicknesses ranging from $0.05r_0$ to $0.2r_0$, where r_0 is the nozzle radius. In what follows, results are provided after a brief description of the simulation parameters and numerical methods. The jets at a Mach number of 0.9 are studied in a first part and those at a Mach number of 0.6 in a second part.

2. PARAMETERS AND METHODS

2.1 Jets parameters

Jets at Mach numbers $\mathrm{M} = u_j/c_0 = 0.6$ and 0.9, where u_j is the jet velocity and c_0 is the ambient speed of sound, impinging on a flat plate located at $6r_0$ from the nozzle-exit plane, are considered. At the nozzle-exit, at $z = 0$, they exhaust from a straight round nozzle into ambient medium at pressure $p_0 = 10^5$ Pa and temperature $T_0 = 293$ K. The nozzle-exit boundary-layers are fully laminar and have thicknesses δ_{BL} equal to $0.05r_0$, $0.1r_0$ or $0.2r_0$, as reported in Table 1. The jet Reynolds number is equal to $\mathrm{Re} = u_j D/\nu = 10^5$, where ν the air kinematic viscosity and $D = 2r_0$ is the nozzle diameter.

Table 1. Jet parameters: Mach number $\mathrm{M} = u_j/c_0$ and nozzle-exit boundary-layer thickness δ_{BL}.

M	0.6	0.6	0.6	0.9	0.9	0.9
δ_{BL}/r_0	0.05	0.1	0.2	0.05	0.1	0.2

2.2 Numerical methods

The large-eddy simulations are carried out using the same framework as in previous impinging jet simulations [9, 14]. They are performed by solving the unsteady compressible Navier-Stokes equations in cylindrical coordinates (r, θ, z) using low-dispersion and low-dissipation explicit schemes. Fourth-order eleven-point centered finite differences are implemented for spatial discretization and a second-order six-stage Runge-Kutta algorithm is used for time integration [15]. A sixth-order eleven-point centered filter [16] is applied explicitly to the flow variables at the end of each time step to remove grid-to-grid oscillations without affecting the wavenumbers accurately resolved, and also to dissipate the kinetic turbulent energy near the grid cut-off frequency. The singularity at $r = 0$ is treated using extra mesh points by applying the method of Mohseni & Colonius [17]. To increase the time step, the derivatives in the azimuthal direction are computed at coarser resolutions than permitted by the grid. Near the plate, for $z > 3r_0$, to avoid the development of high amplitude Gibbs oscillations that can be found near a shock, a shock-capturing filtering procedure based on a shock detector and a second-order filter with reduced errors in the Fourier space is applied to the velocity, pressure and density fluctuations [16]. Non-centered finite differences and filters are used near the pipe walls and the grid boundaries. The radiation conditions of Tam & Dong [18] are applied at the boundaries to avoid significant reflections. A sponge zone combining mesh stretching and Laplacian filtering is also implemented at the boundaries. No-slip and adiabatic wall boundary conditions are imposed to the plate and the pipe walls.

2.3 Computational parameters

The jets are simulated using the same grid, containing $N_r = 559$ points in the radial direction, $N_\theta = 256$ points in the azimuthal direction and $N_z = 1122$ points in the axial direction, yielding a total number of points of 160 millions. It extends radially out to $r = 15r_0$, and axially from $z = -10r_0$ down to the plate, at $z = 6r_0$, excluding the sponge zone which is between $z = -20r_0$ and $z = -10r_0$. In the radial direction, 96 points are used between $r = 0$ and $r = r_0$. The mesh spacing Δr is minimum in the shear layer, at $r = r_0$, where it is equal to $\Delta r_{\min} = 0.0036r_0$. It increases from $r = r_0$ up to $r = 6.2r_0$ where $\Delta r = 0.075r_0$, then is constant up to $r = 15r_0$. The latter mesh spacing leads to a Strouhal number of $\mathrm{St} = fD/u_j = 5.9$, where f is the frequency, for an acoustic wave discretized by five points per wavelength. In the axial direction, the mesh spacing Δz is minimum and equal to $\Delta z_{\min} = 0.0072r_0$ at the nozzle exit. It increases down to $z = 2r_0$, where $\Delta z = 0.12r_0$, then is constant down to $z = 4r_0$, and finally decreases and reaches $\Delta z_{\min}$ again at the plate. The time step is given by $\Delta t = 0.7\Delta r_{\min}/c_0$. In all simulations, the signals of density, velocity and pressure have been recorded at several locations during a time varying from $1700r_0/u_j$ to $2400r_0/u_j$ depending on the jet, after a transient period of $500r_0/u_j$. The Fourier coefficients of the first five azimuthal modes $n_\theta = 0 - 4$ of the flow variables have also been stored. The sampling frequency enables to compute spectra up to $\mathrm{St} = 6.4$. The spectra have been averaged in the azimuthal direction when possible.

2.4 Linear stability analysis

A linear stability analysis is carried out to estimate the variations of the growth rate of the shear-layer instability waves with the Strouhal number. It is performed using the mean flow fields obtained from the large-eddy simulations, with the same techniques as in a previous study by Bogey & Sabatini [13]. For this purpose, the mean flow fields are first interpolated on a uniform grid which extends radially out to $r = 3r_0$ and axially from the nozzle-exit down to the plate, with mesh spacings $\Delta r = 0.00005r_0$ and $\Delta z = 0.05r_0$. The compressible Rayleigh equation is then solved for the axisymmetric mode using a shooting technique [19] for all axial positions. Downstream of the near-nozzle mixing layers, typically between $z = 1.5r_0$ and $z = 3r_0$, the solutions diverge at axial positions which depend on the jet Mach number and the boundary-layer thickness. To evaluate the growth rates at the axial positions where the solutions diverge and further downstream, the growth rates are then approximated using the values obtained at the position of the last converged solution assuming that they scale with the momentum thickness. The growth rates of the damped waves are not evaluated accurately by solving the Rayleigh equation [19]. However, results obtained by Tam & Morris [20] indicate that the growth rates vary approximately linearly with the Strouhal number above the frequency of the neutral shear-layer instability waves. In the present work, the growth rates of the damped waves are therefore approximated using linear extrapolation.

3. RESULTS

3.1 Jets at a Mach number of 0.9

3.1.1 Vorticity and pressure snapshots

To illustrate the influence of the nozzle-exit boundary-layer thickness on the jet development and acoustic radiation, snapshots of vorticity norm and pressure fluctuations are presented for the three jets at $\mathrm{M} = 0.9$ in figure 1. In the vorticity fields, vortex rolling-ups and pairings are observed in all cases. They occur closer to the nozzle exit as the boundary-layer thickness decreases, which leads to a faster development of the mixing layers for the jet with thinner boundary layers.

In the pressure fields, the levels increase for a thicker nozzle-exit boundary layer. For the jet with the thinnest boundary layers in figure 1(a), the pressure field has no clear organization and exhibits both low- and high-frequency waves. For the two jets with the thickest nozzle-exit boundary layers in figures 1(b,c), in contrast, low-frequency acoustic waves originating from the plate are observed. They are characterized by regularly spaced wavefronts symmetrical with respect to the jet axis. Therefore, the jets with $\delta_{\mathrm{BL}} \geq 0.1r_0$ produce a strong tonal axisymmetric noise.

3.1.2 Near-nozzle pressure spectra

The pressure spectra computed at $z = 0$ and $r = 1.5r_0$ are plotted as a function of the Strouhal number in figure 2. In all cases, numerous peaks emerge at frequencies which are very similar for the three nozzle-exit boundary-layer thicknesses. The strongest peaks are obtained at Strouhal numbers $\mathrm{St} \simeq 0.32$, 0.41, 0.68 and 0.82. The dominant peak, at $\mathrm{St} \simeq 0.41$, is associated with the axisymmetric mode and is named A_1. It emerges from the broadband noise by 11 dB for $\delta_{\mathrm{BL}} = 0.05r_0$, and much more strongly, by more than 26 dB, for $\delta_{\mathrm{BL}} \geq 0.1r_0$. Moreover, the amplitude of this peak strongly increases for a thicker nozzle-exit boundary layer. It increases by 20 dB between $\delta_{\mathrm{BL}} = 0.05r_0$ and $\delta_{\mathrm{BL}} = 0.1r_0$, and by 8 dB between $\delta_{\mathrm{BL}} = 0.1r_0$ and $\delta_{\mathrm{BL}} = 0.2r_0$. For the jets with $\delta_{\mathrm{BL}} \geq 0.1r_0$, peaks at the frequency of the first two harmonics of the strongest peak are also observed for $\mathrm{St} \simeq 0.82$ and 1.23. Their amplitudes are higher for a thicker boundary layer. The peak at $\mathrm{St} \simeq 0.32$ is also associated with the mode $n_\theta = 0$ and is named A_2. It emerges strongly from the broadband noise for the jets with $\delta_{\mathrm{BL}} = 0.05r_0$ and $\delta_{\mathrm{BL}} = 0.2r_0$, and more weakly for the jet with $\delta_{\mathrm{BL}} = 0.1r_0$. Its amplitude increases by

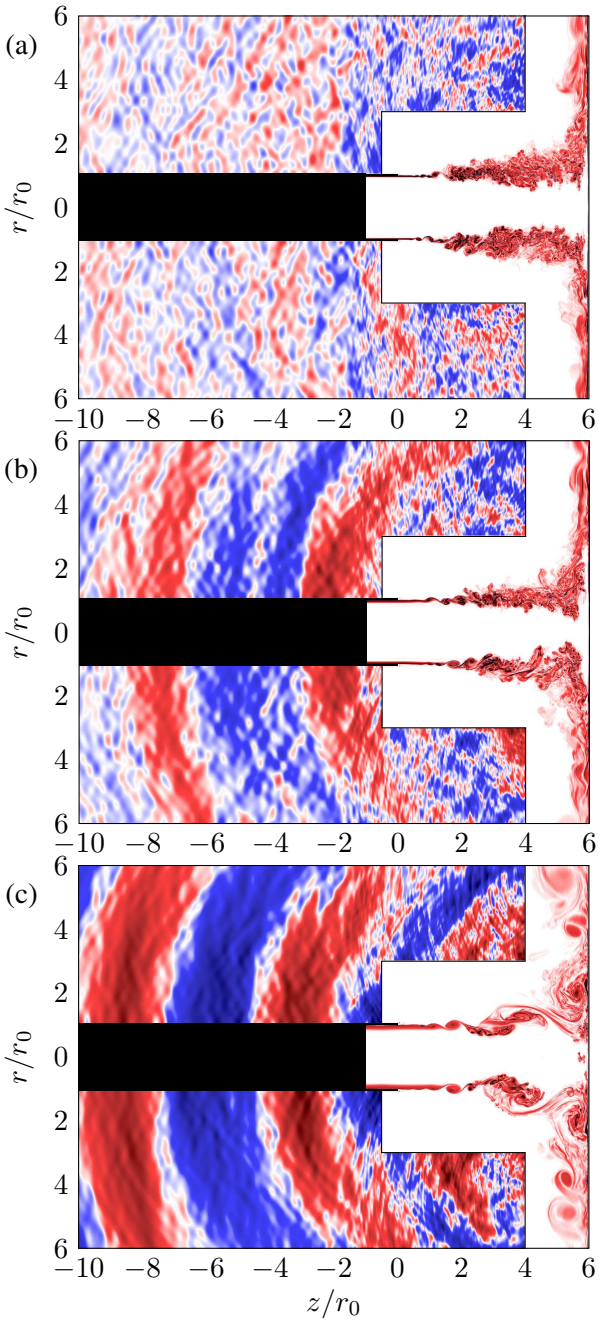

Figure 1. Snapshots in the (z, r) plane of vorticity norm in the flow and of pressure fluctuations outside for the jets at $\mathrm{M} = 0.9$ with (a) $\delta_{\mathrm{BL}} = 0.05r_0$, (b) $\delta_{\mathrm{BL}} = 0.1r_0$ and (c) $\delta_{\mathrm{BL}} = 0.2r_0$. The color scales range between $\pm 20u_j/r_0$ for vorticity, and between $\pm 0.02p_0$ for pressure, from blue to red.

4 dB between $\delta_{\mathrm{BL}} = 0.05r_0$ and $\delta_{\mathrm{BL}} = 0.1r_0$, and by 14 dB between $\delta_{\mathrm{BL}} = 0.1r_0$ and $\delta_{\mathrm{BL}} = 0.2r_0$. The third peak, at $\mathrm{St} \simeq 0.68$, is associated with the first helicoidal mode and is named H_1. Its amplitude increases by 5 dB between $\delta_{\mathrm{BL}} = 0.05r_0$ and $\delta_{\mathrm{BL}} = 0.1r_0$, and decreases by 3 dB between $\delta_{\mathrm{BL}} = 0.1r_0$ and $\delta_{\mathrm{BL}} = 0.2r_0$.

The lowest cut-off frequencies of the free-stream upstream-propagating guided jet waves for $n_\theta = 0$ and $n_\theta = 1$ are also indicated in figure 2. In agreement with previous studies [3, 9, 11], the frequencies of the peaks A_1 and H_1 are very close to these frequencies, for $n_\theta = 0$ and $n_\theta = 1$, respectively. This is not the case for the peak A_2, which may explain why this peak is less strong than the peak A_1.

3.1.3 Power gains of the shear-layer instability waves

The tone amplitudes are likely to vary with the gain in amplitude of the shear-layer instability waves developing between the jet nozzle and the plate at the tone frequencies. In an attempt to explain the variations of the sound levels with the boundary-layer thickness, this gain is thus estimated. It is approximated by

$$G\left(\mathrm{St}\right) = \exp\left(\int_{z_1}^{z_2} -k_i\left(z, \mathrm{St}\right)\, \mathrm{d}z\right), \qquad (1)$$

where $-k_i\left(z, \mathrm{St}\right)$ is the growth or decay rate of the shear-layer instability waves obtained by linear stability analysis, and $z_1 = 0.1r_0$ and $z_2 = 5.5r_0$ are arbitrary integration bounds. The variations of the gain with the Strouhal number are presented in figure 3. In all cases, the gain is higher and then lower as the Strouhal number increases. It reaches a maximum at $\mathrm{St} \simeq 0.8$ for $\delta_{\mathrm{BL}} = 0.05r_0$, at $\mathrm{St} \simeq 0.7$ for $\delta_{\mathrm{BL}} = 0.1r_0$, and at $\mathrm{St} \simeq 0.5$ for $\delta_{\mathrm{BL}} = 0.2r_0$. The values obtained at the frequencies of the peaks A_1 and A_2, shown in figure 3, increases for a thicker nozzle-exit boundary layer. Therefore, the amplification of the shear-layer instability waves developing at the tone frequencies between the nozzle and the plate is stronger for thicker boundary layers. This suggests that the increase of the amplitudes of the two dominant peaks is due to a stronger amplification of the shear-layer instability waves. Moreover, in all cases, the gain at the frequency of the peak A_1 is higher than the gain at the frequency of the peak A_2, indicating that the instability waves developing at the frequency of the peak A_1 between the nozzle and the plate are more amplified than those propagating at the frequency of the peak A_2. This can explain why the tone A_1 is stronger than the peak A_2.

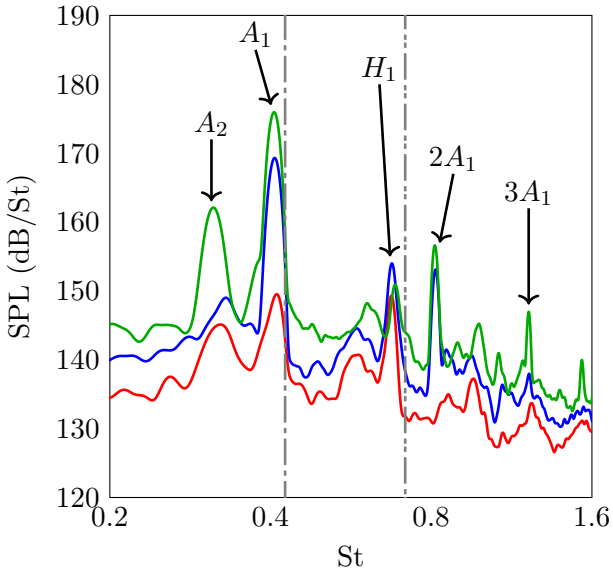

Figure 2. Sound pressure levels (SPL) at $z = 0$ and $r = 1.5r_0$ for the jets at $\mathrm{M} = 0.9$ with $\delta_{\mathrm{BL}} = 0.05r_0$, $\delta_{\mathrm{BL}} = 0.1r_0$ and $\delta_{\mathrm{BL}} = 0.2r_0$, and Strouhal numbers of the lowest cut-off frequency of the free-stream upstream-propagating guided jet waves for $n_\theta = 0$ and $n_\theta = 1$.

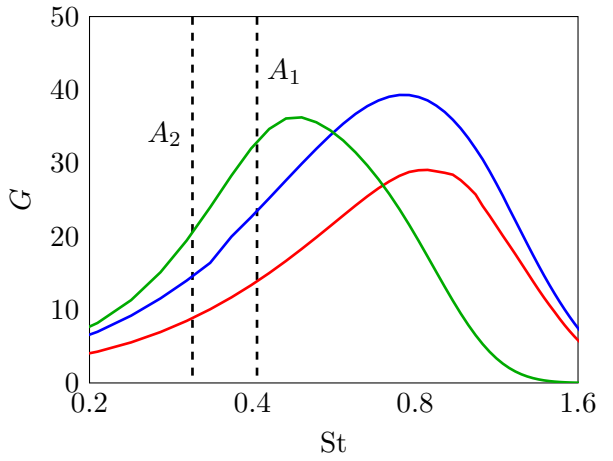

Figure 3. Power gains of the instability waves between $z = 0.1r_0$ and $z = 5.5r_0$ obtained by linear stability analysis for the jets at $\mathrm{M} = 0.9$ with $\delta_{\mathrm{BL}} = 0.05r_0$, $\delta_{\mathrm{BL}} = 0.1r_0$ and $\delta_{\mathrm{BL}} = 0.2r_0$.

3.2 Jets at a Mach number of 0.6

3.2.1 Vorticity and pressure snapshots

Snapshots of vorticity norm and pressure fluctuations are displayed for the jets at $\mathrm{M} = 0.6$ in figure 4. In all cases, the pressure fields do not show a clear organization and exhibit high-frequency acoustic waves of similar amplitudes. In the vorticity fields, vortices appear in the jet shear layers, very close to the nozzle, at $z \simeq 0.5r_0$ for $\delta_{\mathrm{BL}} = 0.05r_0$, at $z \simeq r_0$ for $\delta_{\mathrm{BL}} = 0.1r_0$, and at $z \simeq 2r_0$ for $\delta_{\mathrm{BL}} = 0.2r_0$. Farther downstream, vortex pairings occur. They are located near the nozzle exit for the jets with $\delta_{\mathrm{BL}} \leq 0.1r_0$, and near the plate for the jet with $\delta_{\mathrm{BL}} = 0.2r_0$. For $\delta_{\mathrm{BL}} \leq 0.1r_0$, small-scale vortices are observed downstream of the pairings, indicating that the mixing layers transition to a turbulent state. In contrast, for the jet with the thickest boundary layers, only large-scale vortical structures resulting from the shear-layer rolling-up and vortex pairings are seen to impinge on the plate.

3.2.2 Near-nozzle pressure spectra

The pressure spectra computed at $z = 0$ and $r = 1.5r_0$ are plotted as a function of the Strouhal number in figure 5. For the jet with the thinnest boundary layers, the spectrum is relatively flat, while, for the other jets, a large low-frequency hump is observed around $\mathrm{St} \simeq 0.5$. The hump amplitude is about 10 dB higher for $\delta_{\mathrm{BL}} = 0.2r_0$ than for $\delta_{\mathrm{BL}} = 0.1r_0$. In addition, for $\delta_{\mathrm{BL}} = 0.2r_0$, peaks weakly emerge at Strouhal numbers $\mathrm{St} \simeq 0.35$, 0.5 and 0.77, indicated by dashed lines. They are associated with the axisymmetric mode. The lowest frequency of the least-dispersed guided jet waves, which corresponds to $\mathrm{St} \simeq 1$, also shown, is significantly higher than the peak frequencies.

3.2.3 Standing wave patterns

If the peaks are due to feedback loops, upstream-propagating waves and downstream-travelling waves should lead to constructive and destructive interferences at specific locations in the flow. To determine if such interferences occur, the pressure levels at the three peak frequencies for the axisymmetric mode are shown in the (z, r) plane in figure 6 for the jet with $\delta_{\mathrm{BL}} = 0.2r_0$. In all cases, spots of high energy regularly spaced in the axial direction are observed on both sides of the jet mixing layers, indicating that upstream-propagating waves and downstream-travelling waves result in constructive interferences. The number

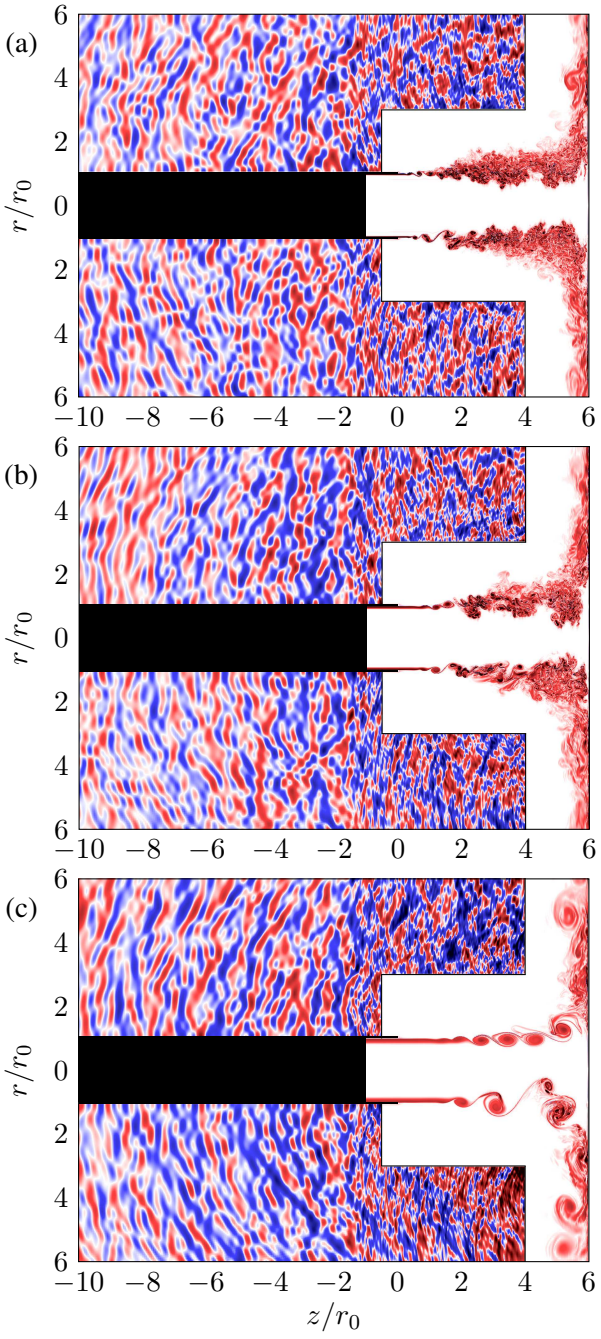

Figure 4. Snapshots in the (z, r) plane of vorticity norm in the flow and of pressure fluctuations outside for the jets at $\mathrm{M} = 0.6$ with (a) $\delta_{\mathrm{BL}} = 0.05r_0$, (b) $\delta_{\mathrm{BL}} = 0.1r_0$ and (c) $\delta_{\mathrm{BL}} = 0.2r_0$. The color scales range between $\pm 20u_j/r_0$ for vorticity, and $\pm 0.005p_0$ for pressure, from blue to red.

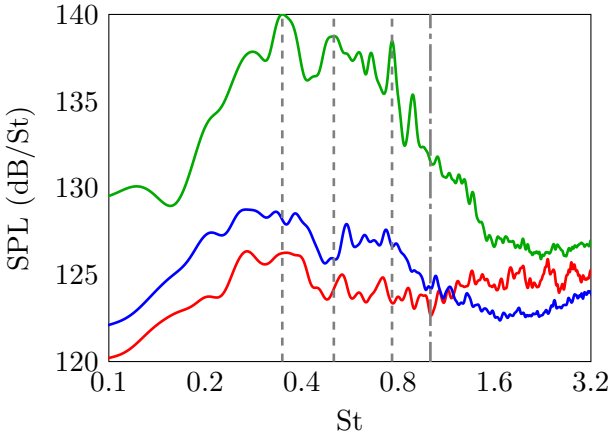

Figure 5. SPL at $z = 0$ and $r = 1.5r_0$ for the jets at M $= 0.6$ with —— $\delta_{\mathrm{BL}} = 0.05r_0$, —— $\delta_{\mathrm{BL}} = 0.1r_0$ and —— $\delta_{\mathrm{BL}} = 0.2r_0$, and Strouhal numbers of - - - - the peaks for $\delta_{\mathrm{BL}} = 0.2r_0$ and —·— the lowest frequency of the least-dispersed guided jet waves.

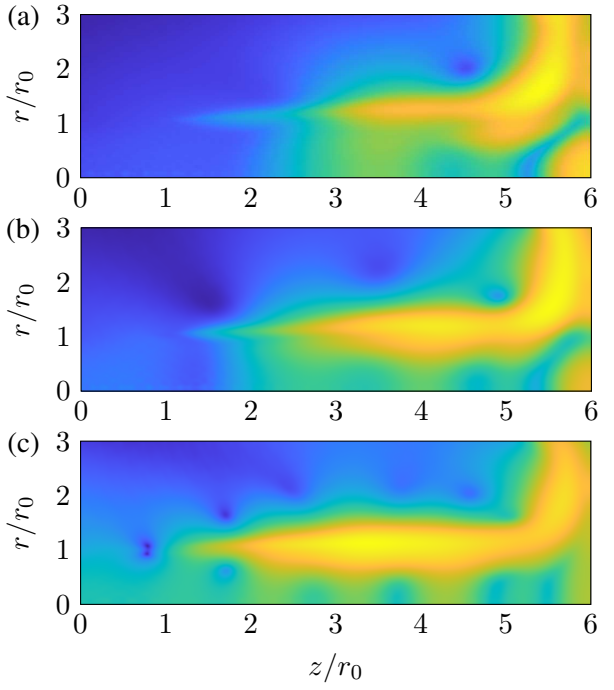

Figure 6. SPL for the jet with $\delta_{\mathrm{BL}} = 0.2r_0$ for $n_\theta = 0$ at (a) St $= 0.35$, (b) St $= 0.5$ and (c) St $= 0.77$. The color scale range between minimum and maximum values, from blue to yellow.

of spots increases with the frequency. Two spots are observed for St $= 0.35$, four for St $= 0.5$ and six for St $= 0.77$. For St $= 0.5$ and St $= 0.77$ in figures 6(b,c), the first and the last spot in the axial direction are found near the nozzle and near the plate, indicating that feedback loops are established between the nozzle and the plate. At these frequencies, the spots below and above the mixing layers are very similar, suggesting that the waves propagating upstream below and above the shear layers travel with the same phase velocities. For St $= 0.5$, the levels are not particularly high near the jet axis, where the amplitudes of the guided jet waves associated with the axisymmetric mode reach their maximum values [10]. In contrast, for St $= 0.77$, the levels are high near the jet axis. These results suggest that the feedback loops are closed by sound waves for St $= 0.5$ and by guided jet waves for St $= 0.77$.

4. CONCLUSION

In this paper, the influence of the nozzle-exit boundary-layer thickness on the noise produced by initially laminar high subsonic impinging jets has been investigated using large-eddy simulations. Jets at Mach numbers of 0.6 and 0.9, with nozzle-exit boundary-layer thicknesses ranging from $0.05r_0$ to $0.2r_0$, have been considered. For the jets at M $= 0.9$, tones have been found in the near-nozzle pressure, at similar frequencies in all cases. The amplitude of the dominant tone is nearly 30 dB stronger for a thicker boundary layer. Results obtained from a linear stability analysis indicate that the rise of the amplitude of the dominant tone is due to a stronger amplification of the shear-layer instability waves developing at the tone frequency for a thicker boundary layer. For the jets at M $= 0.6$, weak peaks are found in the near-nozzle pressure spectrum of the jet with the thickest boundary layers, whereas no peaks are observed for the other jets, suggesting that impinging jets can become resonant as their boundary-layer thickness increases. The results provided in this paper thus show that the boundary-layer thickness may significantly increases the noise produced by impinging jets. However, the influence of the boundary-layer thickness on the noise generated is likely to vary with other jet parameters, such as the nozzle-to-plate distance and the state of the boundary layers. In future studies, it may therefore be interesting to study the effects of the boundary-layer thickness on the noise produced by impinging jets with non-laminar boundary layers and for different nozzle-to-plate distances.

5. ACKNOWLEDGMENTS

The first author was supported by the FUI25 CALM-AA (CiblAge des sources par voie Logicielle et Méthodes inverses pour l'AéroAcoustique) regional project, co-financed by the European regional development fund. This work was granted access to the HPC resources of PMCS2I (Pôle de Modélisation et de Calcul en Sciences de l'Ingénieur de l'Information) of Ecole Centrale de Lyon. It was performed within the framework of the LABEX CeLyA (ANR-10-LABX-0060) of Université de Lyon, within the program Investissements d'Avenir (ANR-16-IDEX-0005) operated by the French National Research Agency (ANR).

6. REFERENCES

[1] G. Neuwerth, "Acoustic feedback of a subsonic and supersonic free jet which impinges on an obstacle," *NASA Tech. Trans. No. F-15719*, 1974.

[2] A. Powell, "The sound-producing oscillations of round underexpanded jets impinging on normal plates," *J. Acoust. Soc. Am.*, vol. 83, no. 2, pp. 515–533, 1988.

[3] V. Jaunet, M. Mancinelli, P. Jordan, A. Towne, D. M. Edgington-Mitchell, G. Lehnasch, and S. Girard, "Dynamics of round jet impingement," in *25th AIAA/CEAS Aeroacoustics Conference*, 2019.

[4] C.-M. Ho and N. S. Nosseir, "Dynamics of an impinging jet. Part 1. the feedback phenomenon," *J. Fluid Mech.*, vol. 105, pp. 119–142, 1981.

[5] J. S. Preisser, "Fluctuating surface pressure and acoustic radiation for subsonic normal jet impingement," *NASA Tech. Paper 1361*, 1979.

[6] D. Edgington-Mitchell, "Aeroacoustic resonance and self-excitation in screeching and impinging supersonic jets – a review," *Int. J. Aeroacoust.*, vol. 18, no. 2-3, pp. 118–188, 2019.

[7] C. Tam and K. Ahuja, "Theoretical model of discrete tone generation by impinging jets," *J. Fluid Mech.*, vol. 214, pp. 67–87, 1990.

[8] P. Panickar and G. Raman, "Criteria for the existence of helical instabilities in subsonic impinging jets," *Phys. Fluids*, vol. 19, no. 10, p. 106103, 2007.

[9] C. Bogey and R. Gojon, "Feedback loop and upwind-propagating waves in ideally expanded supersonic impinging round jets," *J. Fluid Mech.*, vol. 823, p. 562–591, 2017.

[10] C. K. W. Tam and F. Q. Hu, "On the three families of instability waves of high-speed jets," *J. Fluid Mech.*, vol. 201, p. 447–483, 1989.

[11] M. Varé and C. Bogey, "Mach number dependence of tone generation in impinging round jets," in *28th AIAA/CEAS Aeroacoustics 2022 Conference*, 2022.

[12] C. Bogey and C. Bailly, "Influence of nozzle-exit boundary-layer conditions on the flow and acoustic fields of initially laminar jets," *J. Fluid Mech.*, vol. 663, p. 507–538, 2010.

[13] C. Bogey and R. Sabatini, "Effects of nozzle-exit boundary-layer profile on the initial shear-layer instability, flow field and noise of subsonic jets," *J. Fluid Mech.*, vol. 876, p. 288–325, 2019.

[14] M. Varé and C. Bogey, "Generation of acoustic tones in round jets at a mach number of 0.9 impinging on a plate with and without a hole," *J. Fluid Mech.*, vol. 936, p. A16, 2022.

[15] C. Bogey and C. Bailly, "A family of low dispersive and low dissipative explicit schemes for flow and noise computations," *J. Comput. Phys.*, vol. 194, no. 1, pp. 194–214, 2004.

[16] C. Bogey, N. de Cacqueray, and C. Bailly, "A shock-capturing methodology based on adaptative spatial filtering for high-order non-linear computations," *J. Comput. Phys.*, vol. 228, no. 5, pp. 1447–1465, 2009.

[17] K. Mohseni and T. Colonius, "Numerical treatment of polar coordinate singularities," *J. Comput. Phys.*, vol. 157, no. 2, pp. 787–795, 2000.

[18] C. K. Tam and Z. Dong, "Radiation and outflow boundary conditions for direct computation of acoustic and flow disturbances in a nonuniform mean flow," *J. Comput. Acous.*, vol. 04, no. 02, pp. 175–201, 1996.

[19] P. J. Morris, "The instability of high speed jets," *Int. J. Aeroacoust.*, vol. 9, no. 1-2, pp. 1–50, 2010.

[20] C. K. W. Tam and P. J. Morris, "The radiation of sound by the instability waves of a compressible plane turbulent shear layer," *J. Fluid Mech.*, vol. 98, no. 2, p. 349–381, 1980.